Available online at www.sciencedirect.com

ScienceDirect

Energy Procedia 148 (2018) 74–81

Energy Procedia

www.elsevier.com/locate/procedia

73rd Conference of the Italian Thermal Machines Engineering Association (ATI 2018), 12–14 September 2018, Pisa, Italy

Unsteady Methods Applied to a Transonic Aeronautical Gas Turbine Stage

Giorgio Amato[a]*, Matteo Giovannini[a], Michele Marconcini[a], Andrea Arnone[a]

[a]*Department of Industrial Engineering, Università degli Studi di Firenze, Via di Santa Marta 3, 50127 Firenze, Italy*

Abstract

The importance of considering the unsteady effects in aeronautical engine design has brought to the implementation of simplified unsteady CFD models to respect the temporal restrictions of design cycles. A comparison among steady, Non-Linear Harmonic (NLH) and Full-Annulus (FA) methods has been carried out analyzing the transonic turbine stage CT3, experimentally studied at von Karman Institute for Fluid Dynamics. The understanding of the unsteady phenomena is fundamental to increase the engine efficiency and is precluded in steady calculations. As the computational cost of NLH calculations is of the same order of magnitude of steady ones, it represents a valid and competitive option in a turbine design process.

Keywords: transonic turbines; CFD; unsteady, Non-Linear Harmonic, calculation cost

1. Introduction

The aeronautical sector has experienced a period of continuous and strong development for decades. It has had a positive impact on the economy and the welfare state, on the other side it has brought the related environmental impact to be more and more relevant. In order to face this growing problem, the Advisory Council for Aviation Research and Innovation in Europe (ACARE), promoted the editing of the "European Aeronautics: A vision for 2020" [1] first and

* Corresponding author. Tel.: +39-055-275-8797; fax: +39-055-275-8755.
E-mail address: giorgio.amato@unifi.it

10.1016/j.egypro.2018.08.032

then of the "Flightpath 2050" [2]. These documents set the goals the European aeronautical industry should pursue in order to improve flights safety and to become more sustainable from an environmental point of view. Concerning aerodynamics, research and innovation are key aspects in the strategy to reach the targets and, in this context, Computational Fluid Dynamics (CFD) can play a fundamental role in developing new generation airframes and engines. The state-of-the-art aero-engines are designed through CFD tools based on steady-state RANS methods, although more accurate approaches already exist [3]. As DNS and LES are used to investigate only flow-field details, because of their computational requirements, U-RANS Full-Annulus (FA) method is already exploited in stage, and even turbine, analyses. However, FA is very costly and time-consuming, especially for design cycle schedules [4], [5]. FA must solve the whole row, without spatial computational domain reduction. Furthermore, the calculation must consider a full revolution and several periods must be performed to reach the flow periodicity. For this reason, numerous simplified U-RANS methods have been developed. Unsteady phenomena in turbomachinery can be considered of two types: deterministic or stochastic. The latter are related to flow-field instabilities, whereas the former derive from the interaction between fixed and rotating rows and are function of rotational velocity and blade number. All the simplified approaches are based on the hypothesis that the stochastic unsteady effects are negligible in comparison to the deterministic ones and thus, they can be ignored without relevantly affecting the result accuracy. With this assumption, the flow turns periodic and the solution of the whole row can be obtained from the solution of a single vane. Several Fourier-based approaches, whether in time domain or frequency one, have been proposed in the available literature and a detailed review of such methods can be found in [6]. A relevant group exploits the spectral decomposition of periodic flow fluctuations, which are solved through Fourier series, separately from governing equations. Steady flow and perturbation solutions are then composed to obtain the unsteady one. The Non-Linear Harmonic (NLH) approach belongs to this group. It is formulated in the frequency domain, where Navier-Stokes (N-S) equations are not function of time and can be solved in the steady-state with a great advantage in terms of calculation time requirement. The N-S equations average produces non-linear terms, which are directly solved in the perturbation equations set. Thus, an interdependence exists between the two equation sets, which need iterative calculations to reach the whole problem convergence [7]. It is worth to notice that the unsteady solution accuracy depends on two aspects: the validity of the main hypothesis, i.e. the flow-field is dominated by the solved frequencies, and the order of the Fourier series used to model the temporal fluctuations. The NLH method was selected as unsteady simplified method and compared to steady and FA approaches, in terms of solution accuracy and calculation cost. This analysis considered a transonic turbine stage as test-case, in which unsteady and non-linear effects were supposed to be relevant.

2. Turbine Stage

The considered high-pressure transonic turbine stage was tested in the von Karman Institute for Fluid Dynamics short duration compression tube facility CT3 in the framework of the EU TATEF2 project. Dénos et al. [8] reported a detailed test rig and instrumentation description and operating condition parameters as well. The stator row was composed of 43 cylindrical vanes, whereas the rotor one had 64 twisted blades. Both were considered in the uncooled configuration.

Table 1. Main geometrical characteristics.

	C_{ax} (mm)	C_{ax}/h	g/C_{ax}	r_{hub}/r_{tip}	ξ (deg)	N_B
Stator	41.16	0.812	1.313	0.872	54	43
Rotor	39.78	0.738	0.912	0.864	32	64

Tab. 1 lists the main geometrical characteristics of the stage at midspan, where C_{ax} is the axial chord, h is the blade height, g is the row pitch, r is the radius, ξ is the stagger angle and N_B is the blade count number. The test rig was able to reproduce different operating conditions representative of modern high-pressure turbines: three different pressure ratios were considered and the related measurements at midspan are summarized in Tab. 2. The subscripts are related to the measurement planes indices in Fig. 1, which depicts a scheme of the analyzed stage. The rotational speed, the inlet total pressure and temperature were maintained constant for all the considered conditions, respectively 6500 rpm,

165 kPa and 434 K. The axial gap between the stator trailing edge and rotor leading edge was about 40% of the stator axial chord.

Table 2. Operating conditions.

	p_{01}/p_3	Re (x10^6)	$M_{2,is}$	$M_{3rel,is}$
Low	2.42	1.06	1.071	0.65
Nominal	3.86	1.07	1.242	0.97
High	5.12	1.07	1.249	1.18

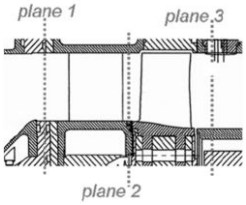

Fig. 1. Schematic representation of the stage CT3 with measurement planes [9].

3. Numerical Set-up

As this work was mainly focused on the employability of a simplified unsteady RANS approach in an industrial design cycle, all CFD analyses reported herein were performed considering tools and models that are usually adopted in an industrial environment. For this reason, a commercial software, i.e. ©Numeca Fine™/Turbo, was selected and for the same reason the Shear-Stress Transport (SST) [10] was used as turbulence model. The boundary conditions (BCs) adopted in the calculations contemplated, as inflow conditions, the measured span-wise distributions of flow angles, total pressure and total temperature. Whereas the radial equilibrium of static pressure was imposed at outlet. The considered inlet turbulence level and turbulent length scale were respectively 5% [11] and 5e-04 m. Fluid and solid walls were modelled respectively as perfect gas and adiabatic surfaces. In steady and NLH calculations the computational domain was composed of one blade passage per row: one stator and one rotor. Periodicity conditions were imposed at boundaries in steady simulations, whereas phase lagged BCs were used in NLH ones to respect the chorocronic periodicity. In all these calculations a non-reflecting model (based on Giles research [12]) was applied at the stator-rotor interface in order to avoid any non-physical reflections. Indeed, it is well known ([13], [14]) that spurious numerical reflections can relevantly worsen the calculation accuracy, when considering transonic stage with low axial gap.

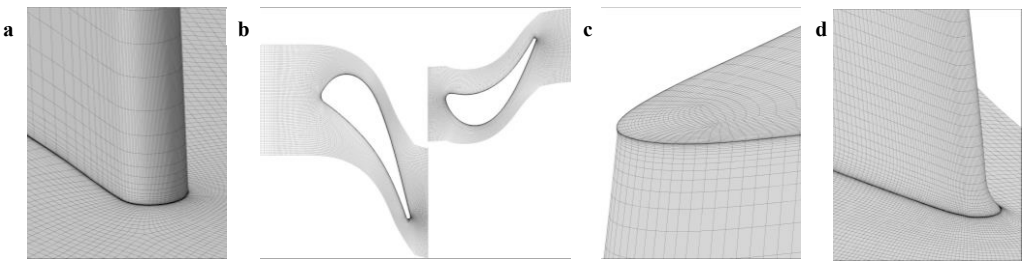

Fig. 2. Fine grid: (a) hub region of stator blade; (b) b2b surface; (c) rotor tip region; (d) rotor fillet.

Computational grids were generated using ©Numeca AutoGrid5™. They were of structured type and O4H topology, which was composed of one O-block around the blade and 4 H-blocks: two respectively on pressure and suction side, one upstream the leading edge and one downstream the trailing edge. The rotor fillet and clearance were modeled: both discretized through a butterfly topology and showed in Fig. 2c and Fig. 2d. Fig. 2b represents a view of the blade-to-blade (b2b) mesh, whereas Fig. 2a depicts a grid detail of the stator trailing edge at hub.

4. Mesh sensitivity

Four different grids were generated to realize the mesh sensitivity analysis, their main characteristics were reported in Tab. 3, in which N_{el}, N_z and N_o are respectively the number of elements of the whole mesh, along the span-wise direction and in the O-block around the blade airfoil in the b2b plane. δ is the first cell width at solid wall.

Table 3. Main parameters of used grids.

	N_{el} (x10^6)	N_z	N_o	δ (x10^{-6}) [m]
Coarse	2	65	294	3.8
Medium	4	81	360	3.0
Fine	6	97	408	2.5
Ultra-Fine	8	113	440	2.1

The adopted minimum wall distances guaranteed an averaged non-dimensionalised minimum wall distance (y^+) smaller than one in all the considered grids, as shown in Fig. 3. Analysing the maximum values of y^+, the range varies in the interval 1.76-1.06 for the stator and 1.51 to 0.88 for the rotor, switching from the Coarse to the Ultra-Fine grid. All these values guarantee a good spatial discretization of the blades laminar sublayer.

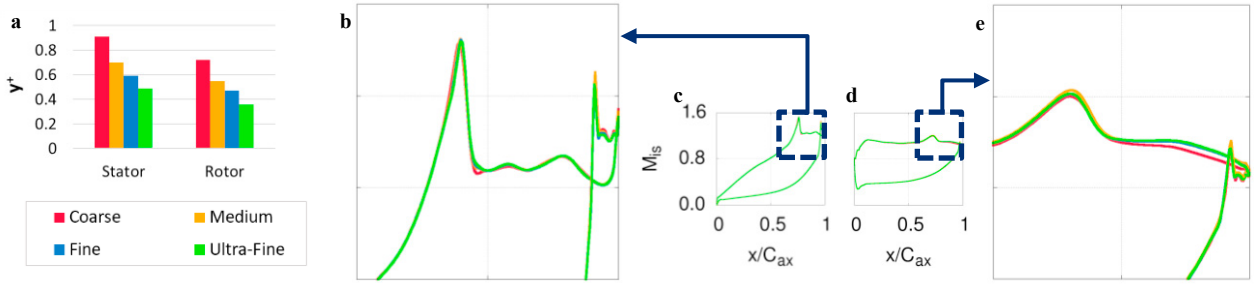

Fig. 3. (a) averaged y^+ on stator and rotor blades; blade load at midspan: (b) stator suction side detail; (c) stator; (d) rotor; (e) rotor suction surface detail.

In terms of global performance, the differences among the simulations are negligible, except for the coarse mesh. Furthermore, Fig. 3c and Fig. 3d show a good agreement of the blade loads among all the different grids. Small discrepancies are observable on the stator suction side (Fig. 3b), near the trailing edge, where the fish tail shock hits the blade surface. More relevant are the differences on the rotor suction side at the trailing edge (Fig. 3e), where the calculated backpressure is lower in the coarse grid analysis with respect to the others. The medium level mesh proved to be sufficiently precise in terms of integral results and blade loads, but a finer discretization allows to better investigate the flow-field details. For this reason, the fine grid was selected to perform all the steady and unsteady calculations showed in the following analyses.

5. NLH calculations

A NLH calculation takes into account only some selected frequencies and their harmonics. Considering a stage environment, the unsteady flow-field of each row is dominated by the adjacent row blade passing frequency, thus only this perturbation was considered in the current activity. In order to select the proper number of harmonics (H), a comparison among four NLH configurations was performed considering the aerodynamic performance and the computational cost in the nominal operating condition. In particular, 1-, 3-, 6- and 12-H were adopted to find the optimum setup in a trade-off between accuracy and computational cost. The first case represents the minimum configuration, the second one is the software default, the third and the fourth ones respect the number of harmonics indicated respectively by Salvadori et al. [15] and Dénos et al. [16].

A comparison among the different configurations is provided in Fig. 4 in terms of isentropic Mach number versus relative axial chord. The 1-H calculation gives lower pressure peaks on the two blade suction sides and relevant discrepancies are observable in Fig. 4a and Fig. 4d. Differently, the 3-, 6- and 12-H configurations show a good agreement especially about the stator fish tail shock description and its effect on the rotor suction side near the leading edge. Focusing on the stator suction surface load, the 6- and 12-H graphs are almost superimposed near the trailing edge, whereas the others show a different pressure field because of a different accuracy in the shock-boundary layer interaction resolution.

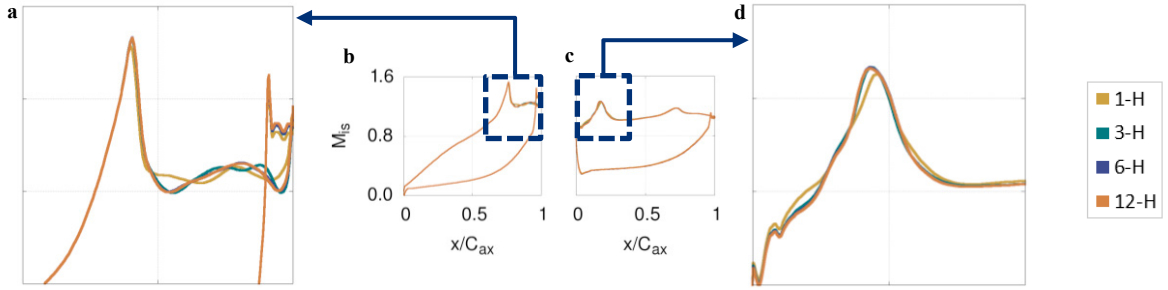

Fig. 4. time-averaged load at midspan: (a) stator suction surface detail; (b) stator; (c) rotor; (d) rotor suction surface detail.

The impact of the harmonic number on the solution looks more relevant analyzing the flow-field. As can be easily observed in terms of instantaneous density gradient (Fig. 5), all the configurations show a black spot on the rotor suction side, near the leading edge. It is the trace of the interaction between the right leg of the stator fish-tail shock and the rotor. Although the 1- and 3-H show this effect, the number of selected harmonics is not sufficient to distinctly represent the shock signal across the stator-rotor interface. The 6- and, clearer, the 12-H display the travelling shock leg, which periodically hits the rotor and causes the density gradient peak near the leading edge.

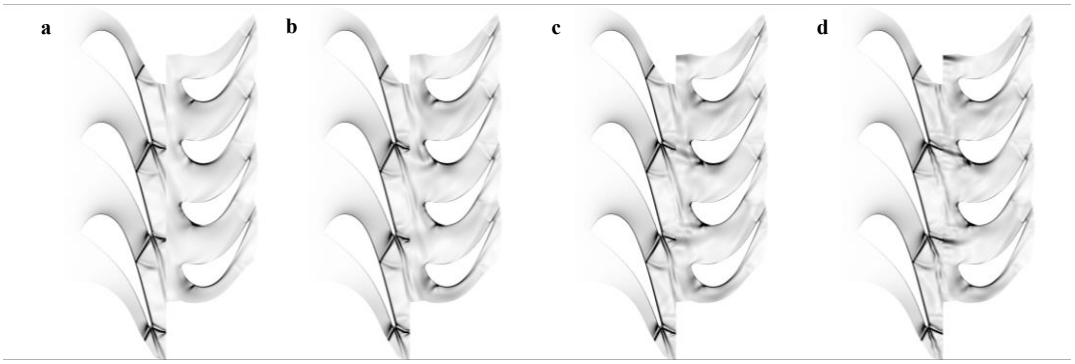

Fig. 5. instantaneous b2b views at midspan of density gradient magnitude at t=0 in the NLH configurations: (a) 1-H; (b) 3-H; (c) 6-H; (d) 12-H.

With respect to the efficiency in Fig. 6a, the graph shows an asymptotic trend increasing the number of modeled harmonics. The efficiency computed in the 1-H configuration is about 0.5% higher than that calculated in the 12-H one, whereas the difference between 6- and 12-H efficiencies is only 0.07%. The calculation cost was measured through two indices, which consider respectively the time and memory requirements. The non-dimensional time (t_{IT}) shown in Fig. 6b represents the ratio between the time needed to perform an iteration in the considered NLH configuration and the time needed by an iteration in the steady calculation. Both are referred to a sequential calculation with an Intel® Core™ i5-6500 CPU @ 3.20 GHz. As the steady and NLH calculations required approximately the same number of iterations to reach the convergence, these ratios are representative of the total calculation time. In the same way, the amount of using RAM was reported in Fig. 6c considering the steady analysis requirement as reference. Both values show a linear increase with the number of modeled harmonics. The 6-H and 12-H show a good agreement from all the examined points of view.

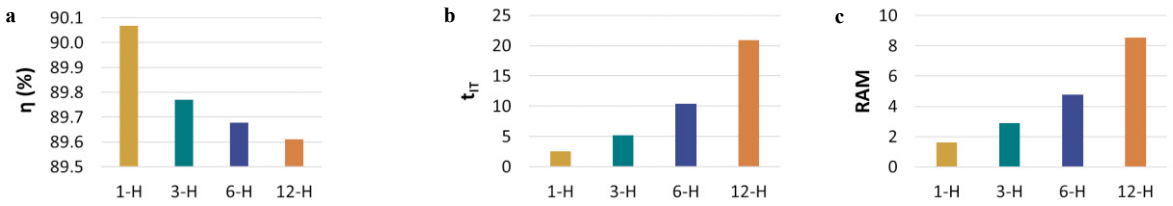

Fig. 6. NLH calculations: (a) turbine isentropic efficiency; (b) steady-related time per iteration; (c) steady-related RAM.

Although the former flow-field solution resolution is lower than the latter one, the 6-H allows to observe the travelling shock through the stator-rotor interface and investigate the interaction between shock and rotor boundary layer. The most relevant difference between the 6- and the 12-H concerns the calculation cost, which is about the 50% in the 6-H configuration. Therefore, the 6-H configuration was selected as optimum to carry out the steady-unsteady and the operating condition comparisons.

6. CFD Methods comparison

The 6-H NLH configuration, selected above, was used to perform a comparison with the steady and the FA analyses to evaluate the differences in terms of solution accuracy and computational cost. The latter represents the unsteady method benchmark, as it is not affected by simplifying hypotheses. Considering the time-averaged stator load in Fig. 7a, a good agreement exists between all the methods, even though some discrepancies are observable around the M_{is} peak, where both the NLH and steady results do not exactly match the FA one. After the shock, instead, the NLH shows a very similar trend to the FA. On the contrary, the steady curve shows more discrepancies, assessing a constant pressure up to the trailing edge.

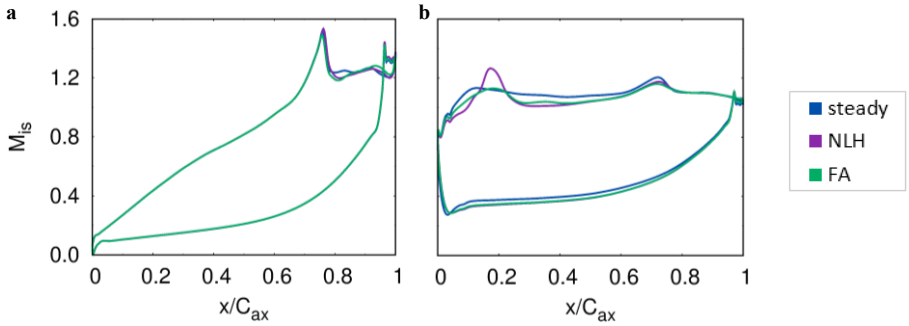

Fig. 7. time-averaged blade load: (a) stator; (b) rotor.

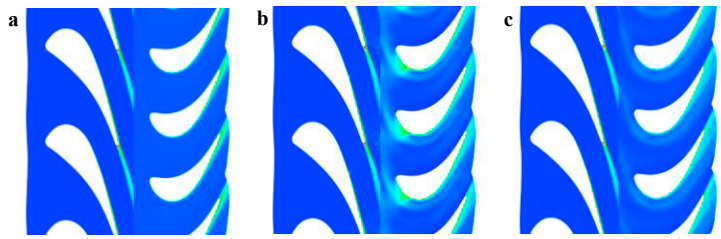

Fig. 8. b2b view of time-averaged entropy at midspan: (a) steady; (b) NLH; (c) FA.

With respect to the time-averaged rotor load (Fig. 7b), differences are more relevant, especially in the shock description near the leading edge. The steady calculation doesn't predict any shock near the leading edge, whereas a strong shock is visible near the 80% of the chord. Furthermore, the pressure level is lower than that prescribed by the unsteady methods all over the blade except for the last 25%, where the three graphs are superimposed. A substantial agreement can be observed between the NLH and FA results, even if they predict a different impact of the stator shock on the rotor leading edge. The NLH approach overestimates this shock with respect to the FA and it causes a higher pressure minimum and higher pressure gradients close to the peak. This difference is mainly due to the effect of those frequencies that were not solved in the NLH calculation. In the FA approach, the proper temporal sampling leads to the resolution of blade passing frequencies and natural ones as well. The complex interaction between the stator shock legs and their reflections on the adjacent stator blade and on the rotor crown as well instantaneously alters the shock impact location on the rotor ([9]). For this reason, observing the time-averaged rotor suction surface load, the M_{is} peak corresponding to the shock near the leading edge looks more spread than the NLH one. The discrepancies about the rotor leading edge shock are confirmed by the entropy b2b views at midspan in Fig. 8. The NLH predicts an entropy peak followed by a less intense region, whereas the FA shows a trace of constant magnitude along the rotor suction

side. In the steady calculation, on the contrary, the entropy is about zero in all the rotor vane. Observing the turbine efficiency (Fig. 9a), the NLH and FA predict similar values, with an difference of about 0.12%, whereas it is about 0.40% between the steady and FA approach. The most important advantage deriving from the use of the NLH approach is linked to its calculation cost reduction with respect to the FA one. Fig 9b shows the calculation time divided by the steady calculation one represented in logarithmic scale to remark the different order of magnitude among steady, NLH and FA analyses: three orders exist between the latter and the other two approaches. As regards the steady-related RAM (Fig. 9c) the discrepancy is much smaller, but consistent nevertheless.

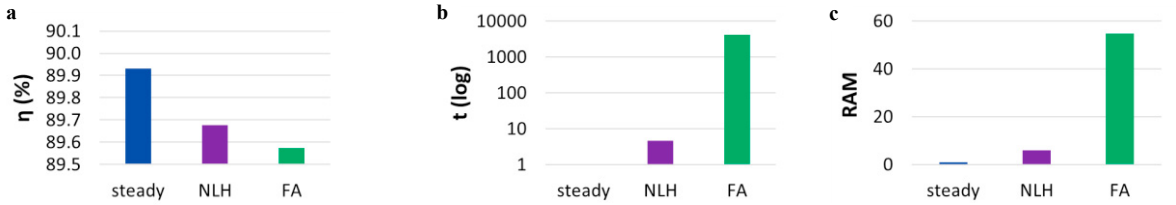

Fig. 9. NLH calculations: (a) turbine isentropic efficiency; (b) steady-related time; (c) steady-related RAM.

The steady analysis doesn't allow to investigate unsteady phenomena at all and leads to relevant errors in integral parameters with regards to the FA approach. On the other hand, the considered unsteady methods show a satisfactory agreement in terms of aerodynamic performance, despite some discrepancies exist, especially with respect to the travelling shock leg impact prediction. Furthermore, considering the consistent calculation cost reduction with respect to the FA method, the NLH approach represents a promising option to the standard steady calculation, even in the first stages of design cycles.

7. Experimental comparison

A comparison between the selected 6-H configuration results and the experimental measures was carried out considering aerodynamic performance in the three aforementioned operating conditions. CFD calculations and experiments are in satisfactory agreement in all the investigated conditions. The nominal and high conditions lead to the same performance in the stator (Fig. 10a) and in the first 60% of the rotor chord (Fig. 10b), as the latter is choked. Span-wise distributions of time-averaged swirl angle (α), total temperature (T_0) and Mach number (M) evaluated at plane 3 are shown in Fig. 10c, Fig. 10d and Fig. 10e. Consistently with other results presented in literature [9] CFD and experimental trends are very similar, even if some differences are observable in the hub region, especially considering the flow angle in the nominal and high conditions. A comparison between calculated and measured values of power and isentropic efficiency was reported on Tab. 4. The overall agreement is satisfactory, even if the CFD consistently under-predicts the efficiency increase switching from the nominal operating condition to the low one. This aspect was already discussed in available literature [17]. The experimental comparison confirms the NLH potentialities in the unsteady investigations. Its capability to resolve the complex flow structures deriving from shock-boundary layer interaction proves to be satisfactory, leading to an accurate stage performance prediction.

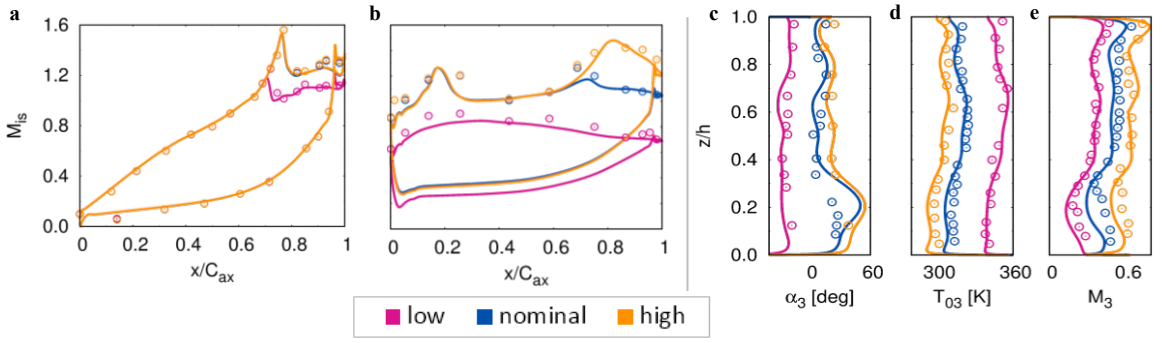

Fig. 10. time-averaged: blade load: (a) stator; (b) rotor; span-wise distributions: (c) swirl angle; (d) total temperature; (e) Mach number.

Table 4. CFD and experimental turbine power at shaft and isentropic efficiency.

	Power [MW]			η (%)		
	Low	Nominal	High	Low	Nominal	High
CFD	0.715	1.011	1.120	90.0	89.7	89.8
EXP	0.713	1.003	1.108	94.8	89.9	90.1

8. Conclusions

The paper presented a comparison among steady, NLH and FA approaches, based on three different aspects: global performance, flow-field analysis and computational cost. The NLH set-up selection went through the harmonic-number sensitivity analysis, which took into account the three parameters explained above. The configuration which modeled six blade passing frequency harmonics proved to be the best compromise between solution accuracy and calculation cost. Both depend on the modeled harmonic number, but the former shows an asymptotic trend, whereas the latter increases linearly. Steady, NLH and FA analyses provided similar solutions in terms of aerodynamic performance. The stator blade load prediction is roughly analogue, whereas the rotor one differs in the description of the shock-blade interaction near the leading edge. The NLH predicted a correlated lower pressure peak with respect to the FA approach, because of a non-resolved complex interaction between the shock and the flow structures located around the stator-rotor interface. Furthermore, the overall agreement of experimental measures and NLH results is satisfactory for all the three investigated operating conditions. Considering the calculation time, three orders of magnitude exist between the FA simulation and the others, whereas the NLH one is less than five times the steady one. In light of these results, NLH proved to be a promising approach and a valid option to the steady one, especially in the first stages of design cycle.

References

[1] EU Commission, Dir.-Gen. for Research and Innovation, “European Aeronautics: A vision for 2020”; (2001) ISBN: 92-894-0559-7.

[2] EU Commission, Dir.-Gen. for Research and Innovation, “Flightpath 2050: Europe’s Vision for Aviation”, (2011) ISBN 978-92-79-19724-6.

[3] Holmes, D. G., Moore, B. J. and Connell, S. D., 2011. “Unsteady vs. steady turbomachinery flow analysis: exploiting large scale computations to deepen our understanding of turbomachinery flows”. In Proc. SciDAC 2011.

[4] Hall, K. C. and Ekici, K. “Multistage coupling for unsteady flows in turbomachinery”. AIAA J 2005; 43: 624–632.

[5] He, L., Chen, T., Wells, R. G., Li, Y. S. and Ning, W. “Analysis of rotor-rotor and stator-stator interferences in multi-stage turbomachines”. *ASME J. of Turbomach.* (2002); vol. 124: 564–571.

[6] He L. Fourier methods for turbomachinery applications. Prog Aerosp Sci 2010; 46: 329–341.

[7] Vilmin, S., Lorrain, E., Hirsch, C. and Swoboda, M. “Unsteady flow modeling across the rotor/stator interface using the nonlinear harmonic method”, ASME Paper GT-2006, 2006.

[8] Dénos, R., Sieverding, C. H., Arts, T., Brouckaert, J.-F., Paniagua, G., Michelassi, V. "Experimental Investigation of the Unsteady Rotor Aerodynamics of a Transonic Turbine Stage." *IMechE J. Power Energy* (1999); vol. 213.

[9] Paniagua, G., Yasa, T., de la Loma, A., Castillon, L. and Coton, T. "Unsteady Strong Shock Interactions in a Transonic Turbine: Experimental and Numerical Analysis." *ASME J. of Turbomach.* (2008); vol. 24.

[10] Menter, F. R. "Two Equations Eddy-Viscosity Turbulence Models for Engineering Applications." *AIAA Journal* (1994); vol. 32.

[11] Yasa, T., Paniagua, G., Dénos, R. "Application of Hot-Wire Anemometry in a Blow-Down Turbine Facility." *ASME J. of Engineering for Gas Turbines and Power* (2007); vol. 129.

[12] Giles, M. "Non-Reflecting Boundary Conditions for the Euler Equations." *CFDL-TR-88-1* (1988).

[13] Rubechini, F., Marconcini, M., Giovannini, M., Bellucci, J. and Arnone, A. "Account for Unsteady Interactions in Transonic Stages." *ASME J. of Engineering for Gas Turbine and Power* (2015); vol. 137.

[14] Marconcini, M., Rubechini, F., Arnone, A., Scotti Del Greco, A. and Biagi, R. "Aerodynamic Investigation of a High Pressure Ratio Turbo-Expander for Organic Rankine Cycle Application." *Proceedings of the ASME Turbo Expo* (2012); 8.

[15] Salvadori, S., Martelli, F. and Adami, P. "Development of a P-L Approach for the Numerical Evaluation of Unsteady Flows." *ICFD* (2010).

[16] Dénos, R., Arts, T., Paniagua, G., Michelassi, V. and Martelli, F. “Investigation of the Unsteady Rotor Aerodynamics in a Transonic Turbine Stage”, *ASME J. of Turbomach.* (2001); vol. 123.

[17] Giovannini, M., Marconcini, M., Arnone, A. and Bertini, F. “Evaluation of Unsteady CFD Models Applied to the Analysis of a Transonic HP Turbine”, *IMechE J. Power Energy* (2014); 228(7).